Available online at www.sciencedirect.com
ScienceDirect
Journal of the European Ceramic Society 30 (2010) 2123–2130
www.elsevier.com/locate/jeurceramsoc

Surface strengthening of Ti_3SiC_2 through magnetron sputtering of Mo and Zr and subsequent annealing

Haiping Guo [a,b], Aijun Li [a,b], Jie Zhang [a,b], Lingfeng He [a,b], Yanchun Zhou [a,*]

[a] *Shenyang National Laboratory for Materials Science, Institute of Metal Research, Chinese Academy of Sciences, 72 Wenhua Road, Shenyang 110016, China*
[b] *Graduate School of Chinese Academy of Sciences, Beijing 100039, China*

Received 19 March 2009; received in revised form 14 April 2009; accepted 18 April 2009
Available online 24 April 2010

Abstract

Magnetron sputtering deposition of Mo and Zr and subsequent annealing were conducted with the motivation to modify the surface hardness of Ti_3SiC_2. For Mo-coated Ti_3SiC_2, Si diffused outward into the Mo layer and reacted with Mo to form molybdenum silicides in the temperature range of 1000–1100 °C. The $MoSi_2$ layer, however, cracked and easily spalled off. For Zr-coated Ti_3SiC_2, Si also diffused outward to form Zr–Si intermetallic compounds at 900–1100 °C. The Zr–Si compounds layer had good adhesion with Ti_3SiC_2 substrate, which resulted in the increased surface hardness.
© 2010 Elsevier Ltd. All rights reserved.

Keywords: Ti_3SiC_2; Surface strengthening; Magnetron sputtering; Microhardness

1. Introduction

Ti_3SiC_2 is one of the $M_{n+1}AX_n$ phases ($n = 1$–3), where M is an early transition metal, A is an A-group element (usually group IIIA–IVA elements), and X is C or N. Ti_3SiC_2 combines unique properties of both metals and ceramics, such as high thermal and electrical conductivity, high elastic modulus and strength, good oxidation resistance and easy machinability.[1–14] However, compared with traditional binary carbides such as TiC, its hardness and wear resistance are relatively low, which limit its widespread applications. Therefore, strengthening by modifying the surface properties of Ti_3SiC_2 without losing its intrinsic merits is of vital importance.

It is well known that the crystal structure of Ti_3SiC_2 can be considered as two-dimensional closed packed layers of Si periodically intercalated into the (1 1 1) twin boundary of $TiC_{0.67}$ (Ti_3C_2).[15] The de-intercalation of Si from Ti_3SiC_2 caused the topological transformation from hexagonal Ti_3SiC_2 to cubic $TiC_{0.67}$. Obviously, when the de-intercalation takes place, the as-formed TiC_x will increase the surface hardness of Ti_3SiC_2. Thus we can induce the topological transformation on the surface of Ti_3SiC_2, which takes place when it reacts with Cu,[16] Ni,[17] graphite,[18] molten cryolite[19] and liquid Al[20] to enhance the surface hardness. In our previous work,[21] magnetron sputtering of Cu and subsequent annealing was used to enhance the surface hardness of Ti_3SiC_2 from 5.08 GPa to a maximum 9.65 GPa owing to the formation of TiC_x following the reaction $Ti_3SiC_2 + 3Cu \rightarrow 3TiC_{0.67} + Cu_3Si$. Nevertheless, the inward diffusion of Cu along the grain boundaries and defects in Ti_3SiC_2 was too fast to maintain a thin and hard surface layer. One possible solution for this problem is to replace Cu with more stable elements such as Mo and Zr. Mo and Zr were chosen because of the following reasons. Similar to the situation of Cu, molybdenum and zirconium silicides are possibly formed by the reaction of Mo and Zr with Ti_3SiC_2.[22,23] The disilicide $MoSi_2$, which exhibits low density (6.24 g/cm^3), high hardness (9.8 GPa, twice that of Ti_3SiC_2), high melting point (2020 °C), and outstanding oxidation resistance up to 1700 °C, is widely used as heating element in high-temperature air furnaces.[24] For zirconium silicide, $ZrSi_2$ has relatively low density (4.89 g/cm^3), high hardness (9.42 GPa), and high melting point (1680 °C).[25,26] In particular, zirconium silicides Zr_xSi_y have been considered as candidates for neutron reflectors (driving back electrons to the

* Corresponding author at: High-performance Ceramic Division, Shenyang National Laboratory for Materials Science, Institute of Metal Research, Chinese Academy of Sciences, 72 Wenhua Road, Shenyang 110016, China.
Tel.: +86 24 23971765; fax: +86 24 23891320.
E-mail address: yczhou@imr.ac.cn (Y. Zhou).

0955-2219/$ – see front matter © 2010 Elsevier Ltd. All rights reserved.
doi:10.1016/j.jeurceramsoc.2009.04.042

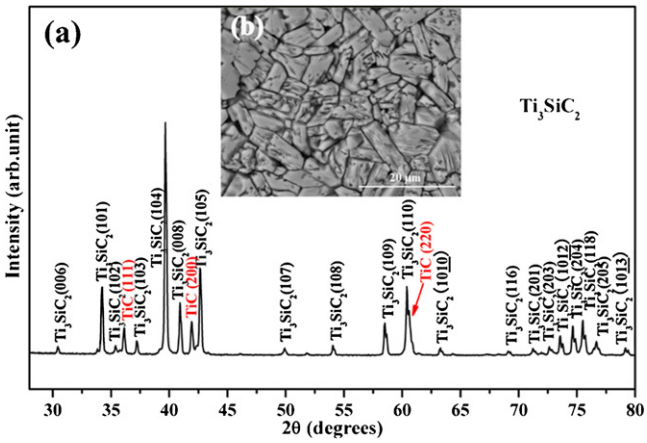

Fig. 1. (a) X-ray diffraction patterns of Ti_3SiC_2 substrate with a little amount of TiC, (b) microstructure of the as-prepared bulk Ti_3SiC_2.

core to increase the reactor's performance) according to simulations based on the elastic scattering cross-section of Si and Zr.[27] Hence, if molybdenum and zirconium silicides were formed on the surface of Ti_3SiC_2, the surface mechanical properties would be improved. The aim of this work is to elucidate the reaction and diffusion mechanisms of Mo and Zr coated on Ti_3SiC_2, and to investigate any strengthening effect brought about by subsequent annealing of the coated samples.

2. Experimental procedures

Bulk Ti_3SiC_2 used in this work was fabricated by an in situ hot pressing/solid–liquid reaction process, which has been described in detail elsewhere.[2] According to the X-ray diffraction pattern shown in Fig. 1a, there is a minor amount of TiC in the as-prepared Ti_3SiC_2 substrate. Fig. 1b shows the microstructure of the as-prepared bulk Ti_3SiC_2. The measured density of Ti_3SiC_2 was 97% of the theoretical value, which was determined by the Archimedes' method.

The Ti_3SiC_2 substrate was cut into rectangular specimens of 8 mm × 8 mm × 2 mm by electrical discharge method from an as-fabricated bulk disk. The surfaces used for sputter deposition were ground down to 1500 grade SiC paper, mechanically polished using 1.5 μm diamond paste to ensure a flat and mirror-like surface, and then ultrasonically cleaned in ethanol and acetone individually for 10 min before they were transferred into the sputtering chamber.

A JGP560C14 ultrahigh vacuum (UHV) magnetron sputtering deposition system (SKY Technology Development Co. Ltd, Shenyang, China) was used to deposit polycrystalline Mo and Zr films onto the Ti_3SiC_2 substrate. During deposition, the substrates were kept static with the substrate-to-target separation (d_{s-t}) of 60 mm to ensure an identical condition for each run. The sputtering chamber was evacuated to a base pressure of $\sim 5 \times 10^{-4}$ Pa, and then backfilled with high purity argon to the required pressure of 0.4–0.5 Pa with a gas flow rate of generally 20 sccm. The Mo and Zr film deposition process was carried out under the deposition DC power of 75 W, meanwhile a negative DC bias of 100 V was applied to the substrate. Prior to deposition, the pure molybdenum and zirconium targets were pre-sputtered for 5 min in order to remove the contaminants and oxides on the surface. During the target cleaning, a shield was interposed between the target and the substrate to avoid the substrate contamination. Although there was no deliberate attempt to heat the substrates, the temperature of the films rose as high as ~70 °C during magnetron sputtering as a result of condensing of the sputtered atoms (the heat of condensation plus their kinetic energy).

Table 1
Parameters for the deposition of Mo and Zr on Ti_3SiC_2 by magnetron sputtering method.

Target source	Mo (Φ 60 mm)	Zr (Φ 60 mm)
Substrate	Ti_3SiC_2	Ti_3SiC_2
Sputtering gas	Ar	Ar
Base pressure (Pa)	5×10^{-4}	5×10^{-4}
Gas partial pressure (Pa)	0.4–0.5	0.4–0.5
Gas flow rate (sccm)	20	20
DC sputtering power (W)	75	75
Negative DC bias applied to the substrate (V)	100	100
Substrate temperature[a] (°C)	70	70
Substrate–target distance (mm)	60	60
Deposition time (min)	60	60
Deposition rate (μm/min)[b]	0.057	0.054

[a] Although there was no deliberate attempt to heat the substrates, the temperature of the films rose as high as ~70 °C during magnetron sputtering as a result of the condensing of the sputtered atoms—the heat of condensation plus their kinetic energy.

[b] Thickness of the film was measured using a HXD-1000B digital microhardness tester and the growth rate was calculated from the film thickness obtained for a given deposition time.

After sputtering, the Mo and Zr-coated Ti_3SiC_2 were annealed in a temperature range of 1000–1100 °C and 900–1100 °C, respectively, for 60–180 min in a horizontal vacuum tube furnace under a pressure of $\sim 5 \times 10^{-3}$ Pa. The detailed processing parameters are listed in Table 1.

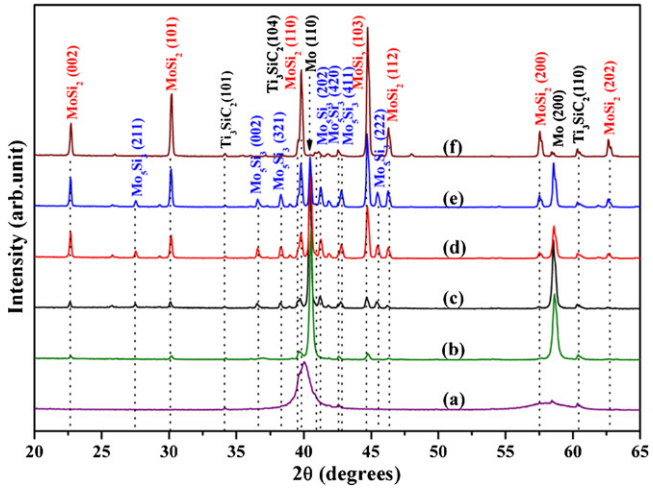

Fig. 2. X-ray diffraction patterns of Mo-coated Ti_3SiC_2 after annealing at (b) 1000 °C for 60 min, (c) 1050 °C for 60 min, (d) 1050 °C for 180 min, (e) 1100 °C for 60 min, and (f) 1100 °C for 180 min. For comparison, diffraction pattern of Mo-coated Ti_3SiC_2 was also listed in (a).

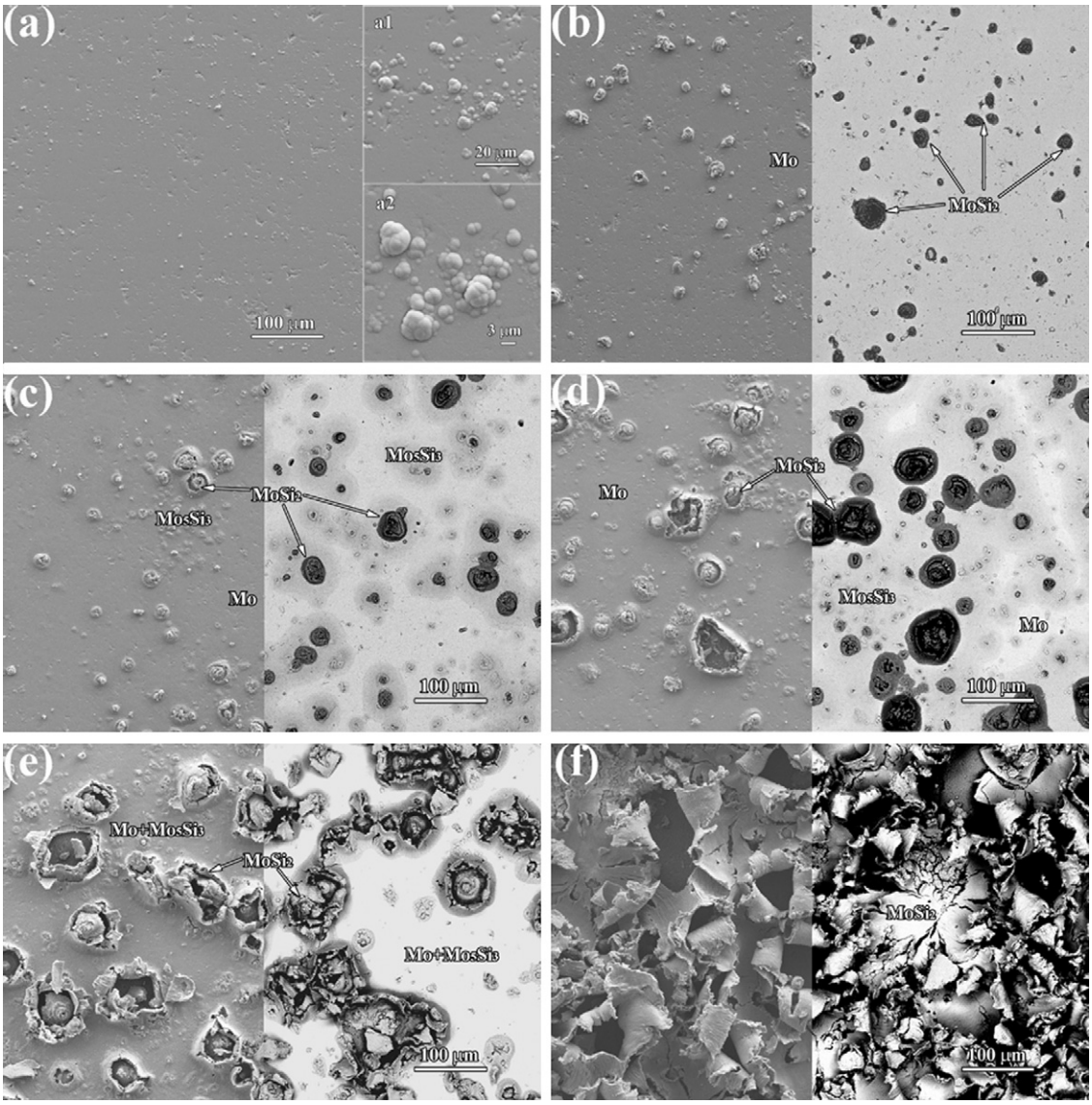

Fig. 3. Surface images of (a) Mo-coated Ti_3SiC_2 and Mo-coated Ti_3SiC_2 after annealing at (b) 1000 °C for 60 min, (c) 1050 °C for 60 min, (d) 1050 °C for 180 min, (e) 1100 °C for 60 min and (f) 1100 °C for 180 min. (Left side: secondary electron images; Right side: back-scattered electron images.)

The modified surfaces were examined by X-ray diffraction (XRD, Rigaku D/max-2400, Japan) with Cu Kα radiation to identify the annealing-induced reaction products. Both the surface and cross-section morphologies of the samples after annealing were examined using a scanning electron microscope (SEM, LEO Super 35, Germany) equipped with an energy dispersive spectroscope (EDS) system. Vickers hardness of the reaction layer was determined by an HXD-1000B digital microhardness tester at a load of 1 N with a dwell time of 15 s. The measured value was the average of ten separate measurements.

3. Results and discussion

3.1. Depositing Mo and subsequent annealing

3.1.1. Phase composition

Fig. 2 shows XRD patterns of Mo-coated Ti_3SiC_2 and those annealed at high temperatures. After sputtering Mo for 60 min, besides diffraction peaks of Ti_3SiC_2, Mo peaks can be observed (Fig. 2a). Indeed, reflections at 2θ values of 40.04°, 58.13° can be assigned as Mo (1 1 0) and Mo (2 0 0), which shifted about 0.5° to low angles compared with those in the JCPDS card No. 42-1120. The most important contribution to XRD peak shifting originated from microstress-induced alteration of the lattice from theoretical value of 3.147 Å to 3.175 ± 0.006 Å, which was calculated from the reflections of Mo-coated Ti_3SiC_2 in Fig. 2a. Moreover, diffraction peaks of Mo were relatively broad, which indicates that there was residual stress in the as-deposited film because of the difference in coefficient of thermal expansion between Mo-coating (α (Mo) = $5.8 \times 10^{-6}\,K^{-1}$) and Ti_3SiC_2 substrate (α (Ti_3SiC_2) = $9.1 \times 10^{-6}\,K^{-1}$).[6,28] It can be seen from Fig. 3a that the surface morphology of Mo-coated Ti_3SiC_2 was relatively flat and tightly packed without voids or gaps and only with an occasional granule which can be clearly seen from the high-magnification images in Fig. a1, a2 (insert in Fig. 3a). After annealing, it can be seen from Fig. 2b–f that all

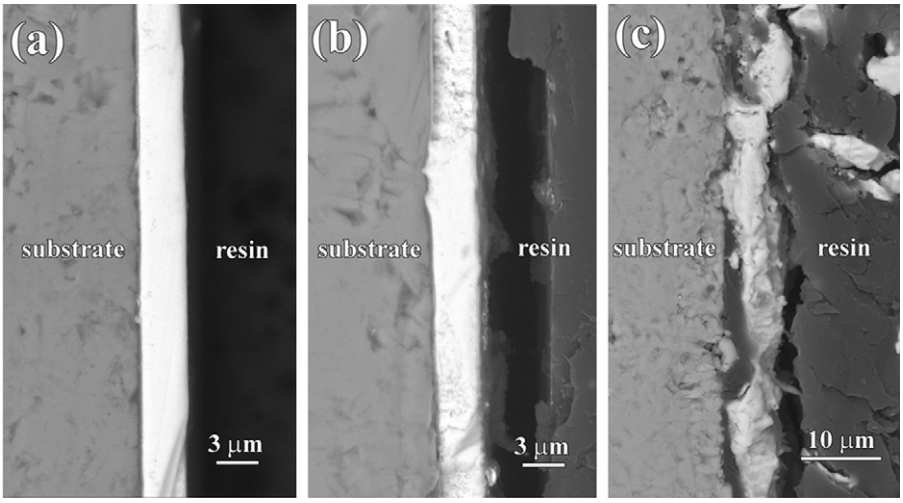

Fig. 4. Back-scattered electron images of cross-sections of Mo-coated Ti_3SiC_2 after annealing at (a) 1000 °C for 60 min, (b) 1050 °C for 60 min, and (c) 1100 °C for 180 min.

the diffraction peaks of Mo shifted to normal positions resulting from the release of microstress. From the XRD patterns, it can be seen that at 1000 °C for 60 min, a small amount of $MoSi_2$ appeared (Fig. 2b). The reaction between Mo and Ti_3SiC_2 can be described as:

$$2Ti_3SiC_2 + (1-x)Mo \rightarrow (1-x)MoSi_2 + 2Ti_3Si_xC_2 \quad (1)$$

Thus, both Mo and $MoSi_2$ existed in the layer. Yoon et al.[29] demonstrated that a columnar Mo_5Si_3 layer could form at the interface between Mo and $MoSi_2$ after heat treating them in the temperature range of 1250–1600 °C owing to the diffusion of Si. In our work, after annealing the Mo-coated film at lower temperature (1050 °C) for 60 min (Fig. 2c), Mo_5Si_3 was detected and the reaction can be expressed as:

$$3MoSi_2 + 7Mo \rightarrow 2Mo_5Si_3 \quad (2)$$

Prolonging the annealing time to 180 min at 1050 °C (Fig. 2d), the amount of $MoSi_2$ increased noticeably and the reflections of Mo_5Si_3 became stronger, while the diffraction peaks of Mo became weaker. Further increasing the annealing temperature to 1100 °C for 60 min (Fig. 2e), reflections of $MoSi_2$ and Mo_5Si_3 increased continuously corresponding to the decrease of Mo peaks. Prolonging the annealing time to 180 min at 1100 °C (Fig. 2f), reflections were mainly assigned to $MoSi_2$. Consequently, the following reaction is proposed for the process:

$$(1-x)Mo_5Si_3 + 7Ti_3SiC_2 \rightarrow 5(1-x)MoSi_2 + 7Ti_3Si_xC_2 \quad (3)$$

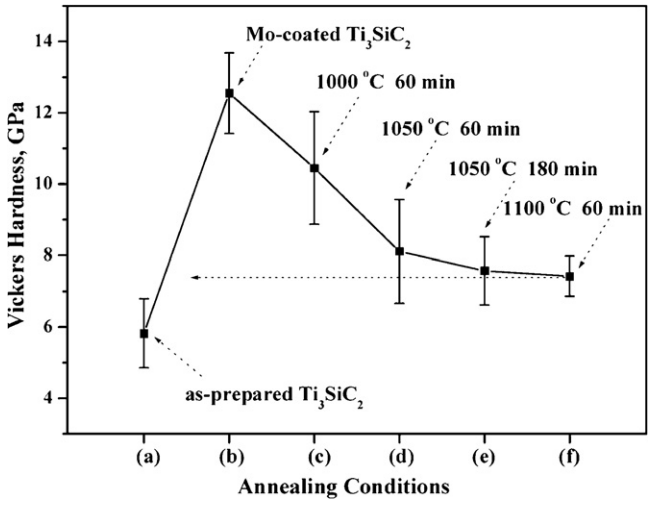

Fig. 5. Microhardness vs. heat treatment conditions, including heat treatment temperature and dwell time, where (a) Ti_3SiC_2 substrate, (b) Mo-coated Ti_3SiC_2, and Mo-coated Ti_3SiC_2 after annealing at (c) 1000 °C for 60 min, (d) 1050 °C for 60 min, (e) 1050 °C for 180 min, (f) 1100 °C for 60 min.

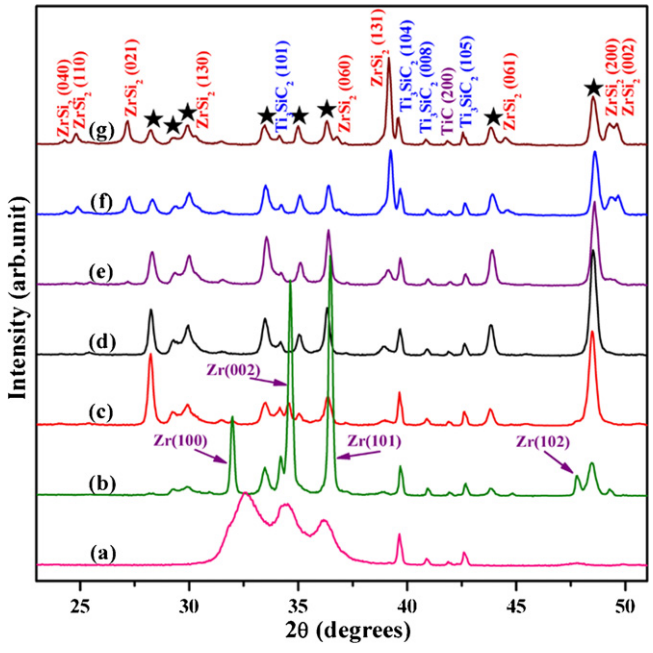

Fig. 6. X-ray diffraction patterns of Zr-coated Ti_3SiC_2 after annealing at (b) 900 °C for 60 min, (c) 950 °C for 60 min, (d) 1000 °C for 60 min, (e) 1050 °C for 60 min, (f) 1100 °C for 60 min, and (g) 1100 °C for 180 min. For convenience in comparison, diffraction pattern of Zr-coated Ti_3SiC_2 was also listed in (a).

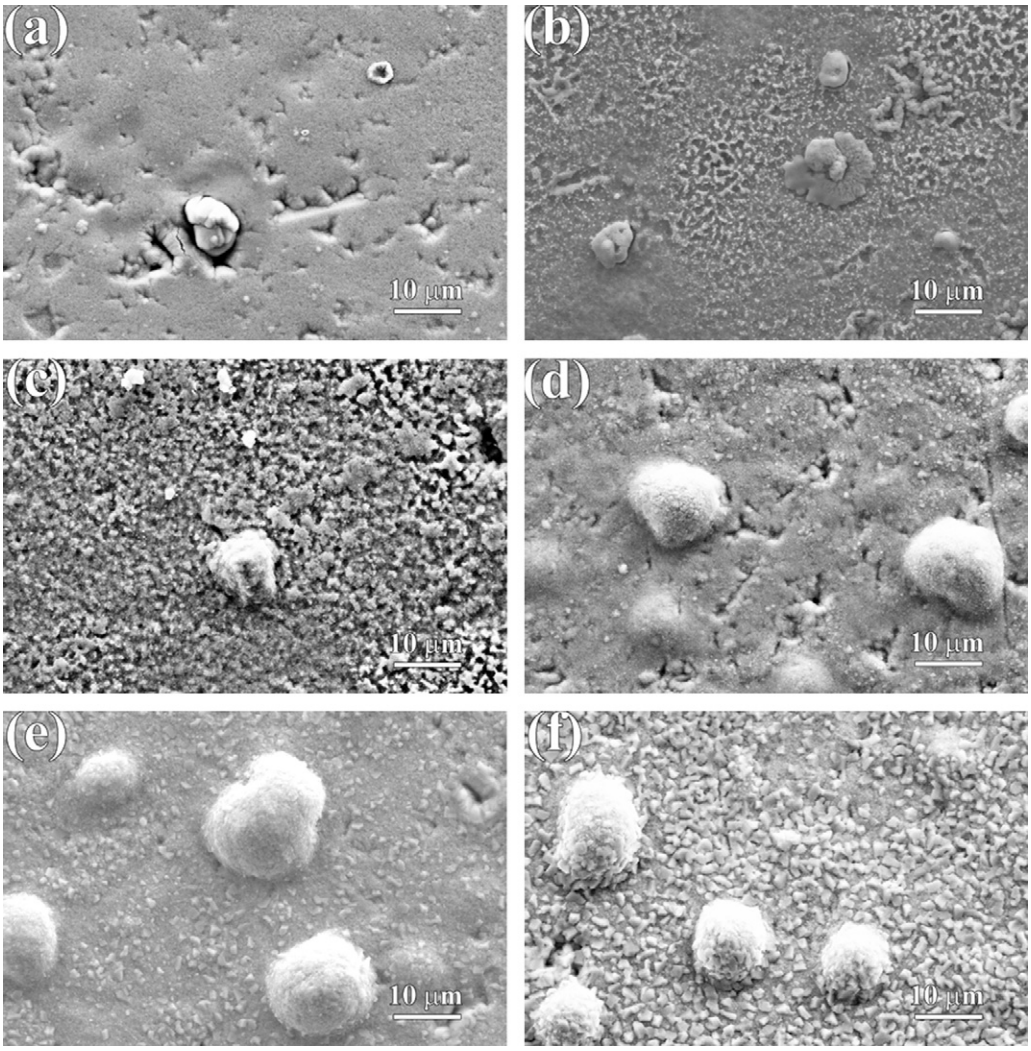

Fig. 7. Surface images of Zr-coated Ti_3SiC_2 after annealing at (a) 900 °C for 60 min, (b) 950 °C for 60 min, (c) 1000 °C for 60 min, (d) 1050 °C for 60 min, (e) 1100 °C for 60 min and (f) 1100 °C for 180 min.

3.1.2. Microstructure

SEM and EDS analyses indicate that surface composition was consistent with the XRD results. Fig. 3b–f shows both secondary and back-scattered electron images of Mo-coated Ti_3SiC_2 after annealing. As shown in Fig. 3b, bulging $MoSi_2$ formed on the surface of Mo-coated Ti_3SiC_2 after annealing at 1000 °C for 60 min. When annealing at 1050 °C for 60 min (Fig. 3c), both the amount and dimension of bulging $MoSi_2$ increased and small Mo_5Si_3 particles appeared around the bulging $MoSi_2$. In addition, the bulging $MoSi_2$ caused cracking. Increasing the temperature and duration, the detachment of $MoSi_2$ further progressed (Fig. 3d, e). At 1100 °C for 180 min (Fig. 3f), the $MoSi_2$ formed on the surface of Ti_3SiC_2 totally split off the Ti_3SiC_2 substrate.

Fig. 4 shows back-scattered electron images of cross-sections of Mo-coated Ti_3SiC_2 after annealing at (a) 1000 °C for 60 min, (b) 1050 °C for 60 min, and (c) 1100 °C for 180 min. At lower temperature (Fig. 4a, b), dense structures with good coating-to-substrate adhesion were obtained. Mo is a relatively stable element which is commonly used as a marker to investigate the diffusion mechanism. From the EDS line scans taken along the layer and its interface with the Ti_3SiC_2 substrate shown in Fig. 4, it can be found that Mo did not diffuse inward, instead Si diffused outward into the Mo layer. But after annealing at 1100 °C for 180 min (Fig. 4c), the coating showed crazing with the formation of $MoSi_2$. In all cases, the same thickness of Mo layer indicated that Mo did not diffuse inward. Consequently, Si diffusing into Mo layer would result in the significant volume increase.

3.1.3. Microhardness

Microhardness under different annealing conditions is shown in Fig. 5. It can be observed from Fig. 5 that the surface of Ti_3SiC_2 was strengthened from 5.08 to 9.65 GPa after sputtering, but the microhardness of the annealed samples decreased with increasing annealing temperature to a steady value of 7.5 GPa. There are two main reasons to explain the phenomenon. First, the change of surface hardness is closely correlated to the compositions on the surface. The hardness of Mo, Mo_5Si_3 and $MoSi_2$ are 15.3, 12.0 and 9.8 GPa,[24,28,30] respectively. The as-coated Ti_3SiC_2 has the highest hardness. After annealing, the amount of

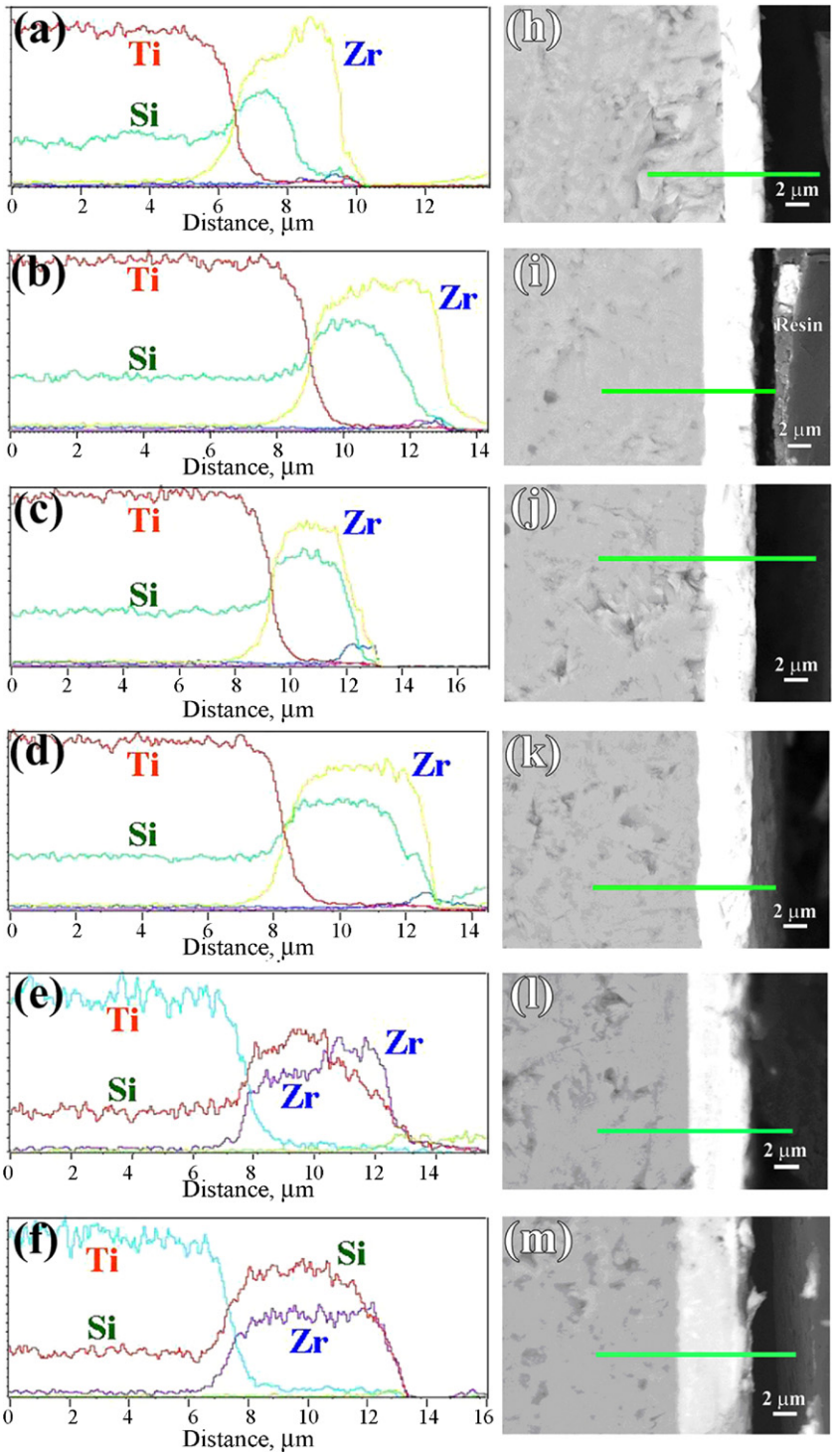

Fig. 8. Line scan and back-scattered electron images of cross-sections of Zr-coated Ti_3SiC_2 after annealing at (a, h) 900 °C for 60 min, (b, i) 950 °C for 60 min, (c, j) 1000 °C for 60 min, (d, k) 1050 °C for 60 min, (e, l) 1100 °C for 60 min and (f, m) 1100 °C for 180 min.

$MoSi_2$ and Mo_5Si_3 increased, which led to the decrease in microhardness. Second, the coating showed crazing with increasing annealing temperature with subsequent disruption of the coating.

Magnetron sputtering Mo and subsequent annealing was intended to strengthen Ti_3SiC_2. However, it did not work due to the cracking of $MoSi_2$ because of the large difference in density between $MoSi_2$, Mo_5Si_3 and Mo-coating (ρ ($MoSi_2$) = 6.24 g/cm^3, ρ (Mo_5Si_3) = 8.24 g/cm^3 and ρ (Mo) = 10.28 g/cm^3).[28,31] The volume increases due to the formation of $MoSi_2$ and Mo_5Si_3 were calculated to be 159% and 45%, respectively. Evidently, the considerable volume increase of $MoSi_2$ led to the detachment. To overcome the cracking of the coating, Zr was deposited on Ti_3SiC_2 and the strengthening effect is described in the following section.

3.2. Depositing Zr and subsequent annealing

3.2.1. Phase composition

Diffraction peaks of Zr can be observed in Fig. 6a after sputtering for 60 min. Similar to the deposition of Mo, the diffraction peaks of Zr were relatively broad and shifted to low angle, which originated from the microstress-induced alteration of lattice. After annealing, diffraction peaks of Zr shifted to their normal positions due to the release of microstress. In addition, besides reflections of Zr, an unidentified Zr–Si phase marked '⋆' appeared after annealing at 900 °C for 60 min (Fig. 6b). Then, the intensity of the unidentified Zr–Si phase increased after increasing the annealing temperature to 1050 °C, meanwhile, the diffraction peaks of Zr became weak (Fig. 6c–e). Further increasing the annealing temperature to 1100 °C (Fig. 6f), $ZrSi_2$ was detected accompanied with the decrease of the unidentified Zr–Si phase. When annealing at 1100 °C for 180 min (Fig. 6g), the amount of $ZrSi_2$ increased. In general, increasing the temperature or prolonging annealing time resulted in the formation of Zr–Si compounds with higher Si content.

3.2.2. Microstructure

Fig. 7 shows surface morphologies of Zr-coated Ti_3SiC_2 under different annealing conditions. At 900 °C for 60 min (Fig. 7a), the Zr-coated surface was relatively flat with some big sputtering particles. Bulging appeared in some area in the sample annealed at 950 °C for 60 min (Fig. 7b), which was identified to be Zr–Si phase by EDS analysis. At 1000 °C for 60 min (Fig. 7c), bulging was extended to the whole surface. Then, some little ridged particles which were determined to be $ZrSi_2$ formed after annealing at 1050 °C for 60 min (Fig. 7d). More ridged particles formed and grew up in the sample annealed at 1100 °C (Fig. 7e). This phenomenon can be clearly seen in Fig. 7f after annealing at 1100 °C for 180 min. The change of surface morphology of Zr-coated Ti_3SiC_2 during annealing was well consistent with the XRD results.

Fig. 8 shows the cross-section microstructure and the EDS line scans results, which reveal an interesting feature. At 900 °C for 60 min, the line scan (in Fig. 8a) taken along the horizontal line in Fig. 8h shows that Si has diffused into one half of the Zr layer. At 950 °C for 60 min (Fig. 8b, i), the diffusion distance of Si has extended to two thirds of the Zr layer. Further increasing the annealing temperature, the diffusion of Si becomes stronger. At 1000 °C (see Fig. 8c, j) and 1050 °C (see Fig. 8d, k), Si has diffused across the whole Zr layer. At these temperatures, the intensity of Si in the line scan spectra is always weaker than that of Zr. But the intensity of Si becomes stronger than that of Zr after annealing at 1100 °C for 60 min (in Fig. 8e, l), which divides the Zr layer into two parts. In the inner part (near Ti_3SiC_2 substrate), the intensity of Si is stronger than that of Zr. In the outer part (surface), the intensity of Si is weaker than that of Zr. After annealing at 1100 °C for 180 min, the intensity of Si exceeds that of Zr in the whole layer. In other words, both the diffusion distance and amount of Si increase with increasing the annealing temperature and dwell time. In addition, the thickness of the layer becomes wider with increasing the annealing temperature and dwell time.

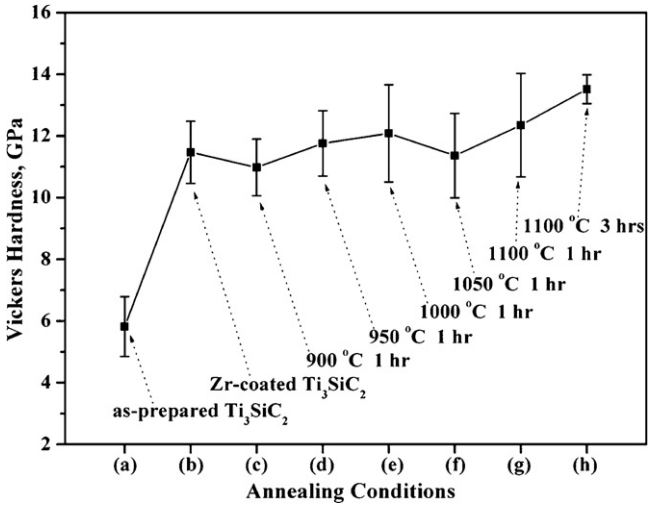

Fig. 9. Microhardness vs. heat treatment conditions, including heat treatment temperature and dwell time, where (a) Ti_3SiC_2 substrate, (b) Zr-coated Ti_3SiC_2, and Zr-coated Ti_3SiC_2 after annealing at (c) 900 °C for 60 min, (d) 950 °C for 60 min, (e) 1000 °C for 60 min, (f) 1050 °C for 60 min, (g) 1100 °C for 60 min, (h) 1100 °C for 180 min.

It is known from the EDS line scan results in Fig. 8 that Zr did not diffuse inward into the Ti_3SiC_2 substrate (analogous to Mo) at the high temperature. Similarly, the reaction was determined by the diffusion of Si. Moreover, the diffusion distance and amount of Si increase with increasing the annealing temperature and dwell time. However, unlike the situation of stable Mo, where the coating thickness was almost constant during the inward diffusion of Si from Ti_3SiC_2 at all annealing conditions, the interface between the Zr–silicide layer and the Ti_3SiC_2 substrate moves with the insert of Si resulting in the increase of layer thickness (Fig. 8a–f), which can release the growth stress resulting from the volume increase. This can explain why no cracking but a good coating-to-substrate adhesion formed in the Zr-coated Ti_3SiC_2 after annealing.

3.2.3. Microhardness

Fig. 9 shows the microhardness of Ti_3SiC_2 substrate and the Zr-coated Ti_3SiC_2 after annealing. It can be clearly seen that the microhardness increased with increasing the annealing temperature and dwell time to a maximum 13.52 GPa at 1100 °C for 180 min. The increase of microhardness is due to increase of the amount of Zr–silicide on the annealed samples and the good adhesion to the Ti_3SiC_2 substrate.

4. Conclusions

Magnetron sputtering Mo and subsequent annealing in the temperature range of 1000–1100 °C were conducted in order to improve the surface hardness of Ti_3SiC_2. During the annealing of Mo-coated Ti_3SiC_2, Mo did not diffuse inward but Si diffused outward into the Mo layer and reacted with Mo to form molybdenum silicides. Due to the big difference in density between $MoSi_2$, Mo_5Si_3 and Mo-coating, the coating showed crazing leading to the invalidation of the coating.

Similarly, magnetron sputtering deposition Zr and subsequent annealing in the temperature range of 900–1100 °C were conducted. Zr did not diffuse inward into the Ti_3SiC_2 substrate at high temperatures. The reaction was determined by the diffusion of Si. Moreover, the diffusion distance and amount of Si increased with increasing annealing temperature and dwell time. At the same time, the interface of Zr–silicide layer moved with the insert of Si leading to an increase of layer thickness, which could release the growth stress resulting from the volume increase. Thus, the as-formed Zr–silicide layer was well coherent with Ti_3SiC_2 substrate resulting in a maximum hardness value of 13.52 GPa.

Acknowledgements

This work was supported by the National Outstanding Young Scientist Foundation (No. 59925208 for Y.C. Zhou), Natural Science Foundation of China under Grant Nos. 50232040, 50302011, 90403027, 50772114, 50832008 and French Atomic Agency (CEA).

References

1. Barsoum MW. The $M_{N+1}AX_N$ phases: a new class of solids; thermodynamically stable nanolaminates. *Prog Solid Chem* 2000;**28**:201–81.
2. Zhou YC, Sun ZM, Chen SQ, Zhang Y. In-situ hot pressing/solid–liquid reaction synthesis of dense titanium silicon carbide bulk ceramics. *Mater Res Innovat* 1998;**2**:142–6.
3. Barsoum MW, El-Raghy T. Synthesis and characterization of a remarkable ceramic: Ti_3SiC_2. *J Am Ceram Soc* 1996;**79**:1953–6.
4. Gao NF, Miyamoto Y, Zhang D. Dense Ti_3SiC_2 prepared by reactive HIP. *J Mater Sci* 1999;**34**:4385–92.
5. Sun ZM, Zhou YC. Ab initio calculation of titanium silicon carbide. *Phys Rev B* 1999;**60**:1441–3.
6. Barsoum MW, El-Raghy T, Rawn CJ, Porter WD, Wang H, Payzant EA, et al. Thermal properties of Ti_3SiC_2. *J Phys Chem Solid* 1999;**60**: 429–39.
7. El-Raghy T, Barsoum MW, Zavaliangos A, Kalidinidi SR. Processing and mechanical properties of Ti_3SiC_2. II. Effect of grain size and deformation temperature. *J Am Ceram Soc* 1998;**82**:2855–60.
8. Li SB, Xie JX, Zhao JQ, Zhang LT. Mechanical properties and mechanism of damage tolerance for Ti_3SiC_2. *Mater Lett* 2002;**57**:119–23.
9. El-Raghy T, Zavaliangos A, Barsoum MW, Kalidinidi SR. Damage mechanisms around hardness indentations in Ti_3SiC_2. *J Am Ceram Soc* 1997;**80**:513–6.
10. Zhou YC, Sun ZM. Microstructure and mechanism of damage tolerance for Ti_3SiC_2 bulk ceramics. *Mater Res Innovat* 1999;**2**:360–3.
11. Zhou YC, Sun ZM, Yu BH. Microstructure of Ti_3SiC_2 prepared by the in-situ hot pressing/solid–liquid reaction process. *Z Metallkd* 2000;**91**:937–41.
12. Sun ZM, Zhou YC, Li MS. High temperature oxidation behavior of Ti_3SiC_2-based material in air. *Acta Mater* 2001;**49**:4347–53.
13. Barsoum MW, El-Raghy T, Ogbuji LUJT. Oxidation of Ti_3SiC_2 in air. *J Electrochem Soc* 1997;**144**:2508–16.
14. Sun ZM, Zhou YC, Li MS. Cyclic-oxidation behavior of Ti_3SiC_2-based material at 1100 °C. *Oxid Metal* 2002;**57**:379–94.
15. Zhou YC, Sun ZM. Crystallographic relations between Ti_3SiC_2 and TiC. *Mater Res Innovat* 2000;**3**:286–91.
16. Zhou YC, Gu WL. Chemical reaction and stability of Ti_3SiC_2 in Cu during high-temperature processing of Cu/Ti_3SiC_2 composites. *Z Metallkd* 2004;**95**:50–6.
17. Yin XH, Li MS, Zhou YC. Microstructure and mechanical strength of diffusion bonded Ti_3SiC_2/Ni joints. *J Mater Res* 2006;**9**:2415–21.
18. El-Raghy T, Barsoum MW. Diffusion kinetics of the carburization and silicidation of Ti_3SiC_2. *J Appl Phys* 1998;**83**:112–9.
19. Barsoum MW, El-Raghy T, Farber L, Amer M, Christini R, Adams A. The topotactic transformation of Ti_3SiC_2 into a partially ordered cubic $Ti(C_{0.67}Si_{0.06})$ phase by the diffusion of Si into molten cryolite. *J Electrochem Soc* 1999;**146**:3919–23.
20. El-Raghy T, Barsoum MW, Sika M. Reaction of Al with Ti_3SiC_2 in the 800–1000 °C temperature range. *Mater Sci Eng A* 2001;**298**:174–8.
21. Guo HP, Zhang J, Li FZ, Liu Y, Yin JJ, Zhou YC. Surface strengthening of Ti_3SiC_2 through magnetron sputtering Cu and subsequent annealing. *J Eur Ceram Soc* 2008;**28**:2099–107.
22. Murarka SP. Transition metal silicides. *Annu Rev Mater Sci* 1983;**13**:117–37.
23. Mayer JW, Tu KN. Analysis of thin-film structures with nuclear backscattering and X-ray diffraction. *J Vac Sci Technol* 1974;**11**:86–93.
24. Mitra R, Khanna R, Rama Rao VV. Microstructure, mechanical properties and oxidation behavior of a multiphase $(Mo,Cr)(Si,Al)_2$ intermetallic alloy-SiC composite processed by reaction hot pressing. *Mater Sci Eng A* 2004;**382**:150–61.
25. Rosenkranz R, Frommeyer G. Microstructures and properties of the refractory compounds $TiSi_2$ and $ZrSi_2$. *Z Metallkd* 1992;**83**:685–9.
26. Ermakov SV, Tsarev BM. Thermoelectric emission of metal silicides from the transition groups of the periodic system of elements. *Radiotekh Electron* 1962;**7**:2101–4.
27. Le Flem Ma, Canel J, Urvoy S. Processing and characterization of Zr_3Si_2 for nuclear applications. *J Alloys Compd* 2008;**465**:269–73.
28. Shackelford J, Alexander W, editors. *CRC materials science and engineering handbook*. Boca Raton, FL: CRC Press Inc.; 1992.
29. Yoon JK, Lee JK, Lee KH, Byun JY, Kim GH, Hong KT. Microstructure and growth kinetics of Mo_5Si_3 and Mo_3Si layers in $MoSi_2$/Mo diffusion couple. *Intermetallics* 2003;**11**:687–96.
30. Chu F, Thoma DJ, McClellan KJ, Peralta P. Mo_5Si_3 single crystals: physical properties and mechanical behavior. In: *High temperature structural silicide meeting*. 1998.
31. Vasudfvan AK, Petrovic JJ. A comparative overview of molybdenum disilicide composites. *Mater Sci Eng A* 1992;**155**:1–17.